Article:
Walling, S.A., Gardner, L.J. orcid.org/0000-0003-3126-2583, Prentice, D.P. orcid.org/0000-0002-4980-8751 et al. (5 more authors) (2023) Stability of SrCO3 within composite Portland-slag cement blends. Cement and Concrete Composites, 135. 104823. ISSN: 0958-9465

https://doi.org/10.1016/j.cemconcomp.2022.104823

Cement and Concrete Composites 135 (2023) 104823

Contents lists available at ScienceDirect

Cement and Concrete Composites

journal homepage: www.elsevier.com/locate/cemconcomp

Stability of $SrCO_3$ within composite Portland-slag cement blends

Sam A. Walling [a], Laura J. Gardner [a], Dale P. Prentice [b,c], Malin C. Dixon Wilkins [a], Adham A. Hammad [a], Wooyong Um [d,e,f], Claire L. Corkhill [a,*], Neil C. Hyatt [a]

[a] Immobilisation Science Laboratory, Department of Materials Science & Engineering, The University of Sheffield, Sheffield, S1 3JD, United Kingdom
[b] Laboratory for the Chemistry of Construction Materials (LC2), Department of Civil and Environmental Engineering, University of California, Los Angeles, CA, United States
[c] Institute for Carbon Management (ICM), University of California, Los Angeles, CA, 90095, USA
[d] Division of Advanced Nuclear Engineering (DANE), Pohang University of Science and Technology (POSTECH), 77 Cheongam- Ro, Nam-GU, Pohang, Gyeongbuk, 790-784, Republic of Korea
[e] Division of Environmental Science and Engineering (DESE), Pohang University of Science and Technology (POSTECH), 77 Cheongam-ro, Nam-Gu, Pohang, Gyeongbuk, 37673, Republic of Korea
[f] Nuclear Environmental Technology Institute (NETI), Pohang, Gyeongbuk, 37673, Republic of Korea

ARTICLE INFO

Keywords:
Strontium
Carbonate
Nuclear
Immobilisation
Reaction
Thermodynamics

ABSTRACT

The stability and reactivity of $SrCO_3$ within a blended Portland-slag cement at both 20 °C and 60 °C (to simulate an indicative waste form for disposal) was determined via XRD, TG-MS, SEM-EDX and thermodynamic modelling. $Sr^{14}CO_3$ is a potential long-term sink for trapping radioactive ^{14}C, produced through the nuclear fuel cycle, therefore understanding its stability in potential cementitious waste forms is of interest and importance. Incorporation of 30 wt% $SrCO_3$ in blended Portland-slag cement caused minor reactions to occur, resulting in increased formation of carbonated AFm phases, along with stabilisation of ettringite at 20 °C, precluded at 60 °C due to the reduced stability to ettringite at this temperature. Thermodynamic modelling predicted only minor $SrCO_3$ reactivity up to 360 days, with carbonate remaining stable over this timeframe, validated by our experimental results. Thus, thermodynamic simulations predict that $SrCO_3$ is an effective immobilisation matrix for ^{14}C, within a blended Portland-slag cement waste form, suitable for long-term geological disposal.

1. Introduction

The safe management of radioactive wastes arising from the nuclear fuel cycle is crucial for clean-up of legacy civil and defence nuclear programmes, and for securing public confidence in civil nuclear energy as a low carbon source of electricity in the context of eliminating CO_2 emissions as part of international climate change commitments [1]. Radioactive wastes are managed at a national level according to various policy and regulatory requirements, which increasingly emphasise the principles of the waste hierarchy, to minimise the quantity of radioactive waste to be disposed [2]. Moreover, there is generally a requirement that radioactive wastes should be treated and packaged so as to be passively safe for long term storage and disposal [3,4].

Carbon-14 (^{14}C) is a potentially challenging radionuclide in the context of the final geological disposal of radioactive wastes. It is a beta emitter (decaying to ^{14}N), has a relatively long half-life (5730 years), and can distribute globally as part of the carbon cycle [5]. Consequently, proposed national waste repositories pay careful consideration to wastes containing concentrated levels of ^{14}C. Though some ^{14}C occurs naturally in the atmosphere from the interaction of cosmic ray neutrons with ^{14}N (by the reaction $^{14}N(n,p)^{14}C$), production of ^{14}C within the nuclear fuel cycle typically occurs via neutron mediated reactions with ^{13}C, ^{14}N, ^{15}N, ^{16}O and ^{17}O which may be present in nuclear fuels, reactor moderators, and primary coolant systems [5,6]. The most significant route to production of ^{14}C in nuclear power plants is via the $^{14}N(n,p)^{14}C$ reaction, due to the very high thermal neutron capture cross-section of ^{14}N, with a natural isotopic abundance of 99.6%. Other significant contributors to ^{14}C generation are the $^{17}O(n,\alpha)^{14}C$ and $^{13}C(n,\gamma)^{14}C$ reactions, the latter being of particular importance in the context of graphite moderated reactors and carbide fuels [5–7].

On average the production of ^{14}C in a conventional light water moderated pressurised water reactor (PWR) is 1480 GBq·GW(e)$^{-1}$·yr^{-1}, with the majority occurring within the fuel and fuel cladding, resulting in peak release of ^{14}C during fuel reprocessing (if undertaken) [5]. A

* Corresponding author.
E-mail address: c.corkhill@sheffield.ac.uk (C.L. Corkhill).

https://doi.org/10.1016/j.cemconcomp.2022.104823
Received 22 October 2021; Received in revised form 26 June 2022; Accepted 19 October 2022
Available online 9 November 2022

Table 1
Batched mix formulations.

	GGBS (g)	PC (g)	$SrCO_3$ (g)	H_2O (g)	w/s ratio
0% mix	180	20	0	78	0.39
30% mix	126	14	60	78	0.39

further portion of ^{14}C will be captured in ion-exchange resins used at the power plants [8]. The generation of ^{14}C is much higher for heavy water moderated reactors (e.g. CANDU reactors), typically being 10^3 GBq·GW(e)$^{-1}$·yr^{-1} with the majority occurring in the coolant/moderator. This leads to an accumulation of ^{14}C within ion-exchange resins used for coolant/moderator purification at these facilities [5,9]. This increased ^{14}C production is due to elevated levels of ^{17}O within the heavy water coolant/moderator resulting in an increased number of $^{17}O(n,\alpha)^{14}C$ reactions [10–12].

The occurrence of radioactive wastes rich in ^{14}C has encouraged research to extract and concentrate the ^{14}C inventory for immobilisation in a waste form suitable for disposal. This route is of particular interest for CANDU reactor operators, where research has been undertaken on the selective stripping of ^{14}C from resins [13,14], or other low temperature treatments [15], allowing residual resins to be classified as low-level waste. However, one remaining issue is how to safely immobilise the extracted ^{14}C into a durable waste form. Within the UK, nuclear fuel reprocessing at the THermal Oxide Reprocessing Plant (THORP, which ended reprocessing in 2018) utilised an off-gas system to reduce radioactive discharges, which removed ^{14}C with an alkaline scrubber, precipitating solid $Ba^{14}CO_3$, which was then sent for on-site cementation within a blended Portland cement [16,17]. Investigation of $BaCO_3$-Portland cement interactions demonstrated the potential for carbonate release due to thermodynamically favourable $Ba^{14}CO_3 + SO_4^{2-} \rightarrow BaSO_4 + {}^{14}CO_3^{2-}$ reactions from sulfate within cements [18], or from sulfates in groundwaters (e.g. post-disposal) [19]. The risk posed by this reaction is mitigated, to some extent, by the use of blended Portland cements (e.g. slag-cement blends) in the UK nuclear industry [18]. Nevertheless, uncertainties remain about long-term stability due to interactions with sulfates from groundwater.

In an industrial setting, free ^{14}C is typically trapped via alkaline scrubbers and precipitated as a less soluble carbonate ($BaCO_3$, $CaCO_3$, etc.), but it can also be trapped via molecular sieves or potentially via direct gas interaction with a substrate (such as $Sr(OH)_2$) [5,20]. Precipitation as an alkaline earth carbonate is favoured due to proven technology, relatively low cost inputs, low solubility and good thermal stability [6]. Some research has also been undertaken on sintering of $BaCO_3$ or $BaCa(CO_3)_2$ waste forms [7,21]. Other carbonates, of lower solubility, are also of interest such as $PbCO_3$, $CdCO_3$ and $ZnCO_3$, but these will decompose at a much lower temperature (<500 °C) releasing carbonate [22].

For disposal in a geological repository, the long-term stability of the carbonate waste form is paramount [23]. For near-neutral conditions, $(BiO)_2CO_3$, $Pb_3(OH)_2(CO_3)_2$ and $MnCO_3$ have been promoted as promising candidates [19]. However, for countries developing geological repositories which will contain significant quantities of cementitious material, higher pH conditions are likely to prevail (such as in several proposed generic UK designs [24]). Under such conditions, the most widely favoured method for trapping ^{14}C is within alkaline earth carbonates due to their particularly low solubility in alkaline conditions. From thermodynamic considerations, only $CaCO_3$ and $SrCO_3$ are resistant to sulfate reactions, with $SrCO_3$ being the least soluble [6,22,25]. Therefore, the use of $SrCO_3$ as the ^{14}C immobilisation matrix in a cement encapsulated waste form, would improve the long-term safety function. Remarkably, however, this optimisation has been largely overlooked and the potential interaction of $SrCO_3$ within a cementitious environment is uncertain.

Much of our understanding of the interaction of Portland cement with alkaline earth carbonates is based on $CaCO_3$-cement interactions,

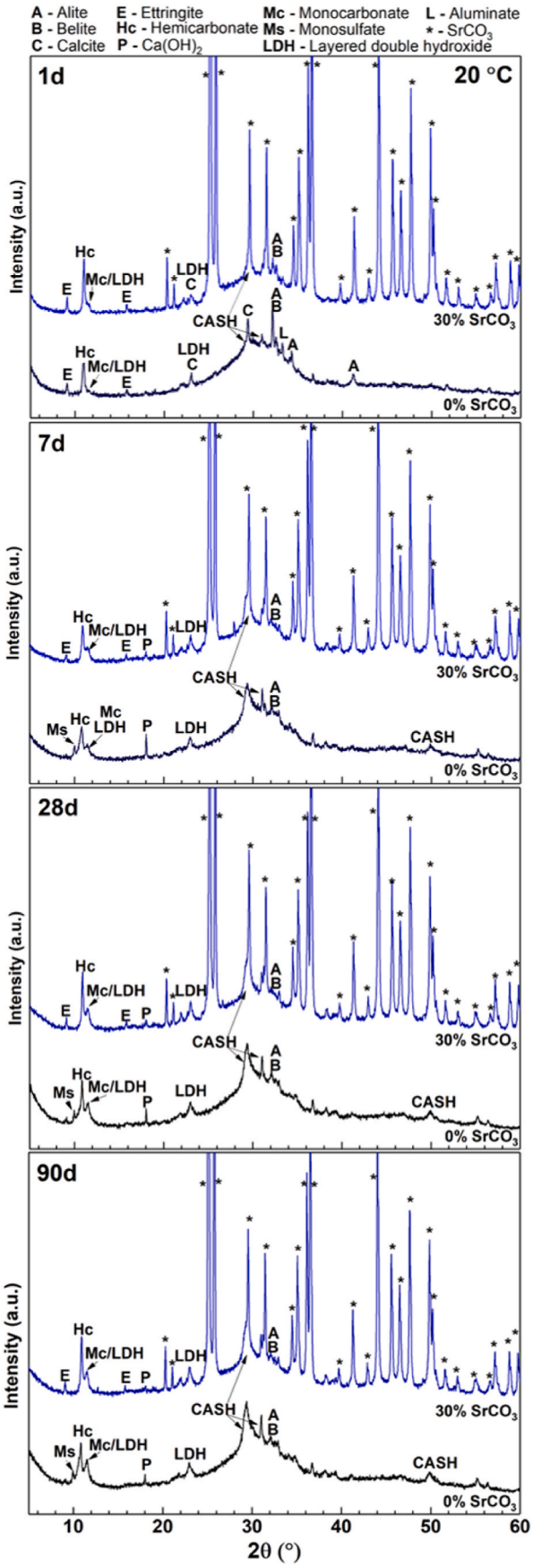

Fig. 1. X-ray diffraction patterns of samples cured at 20 °C from 1 day through to 90 days.

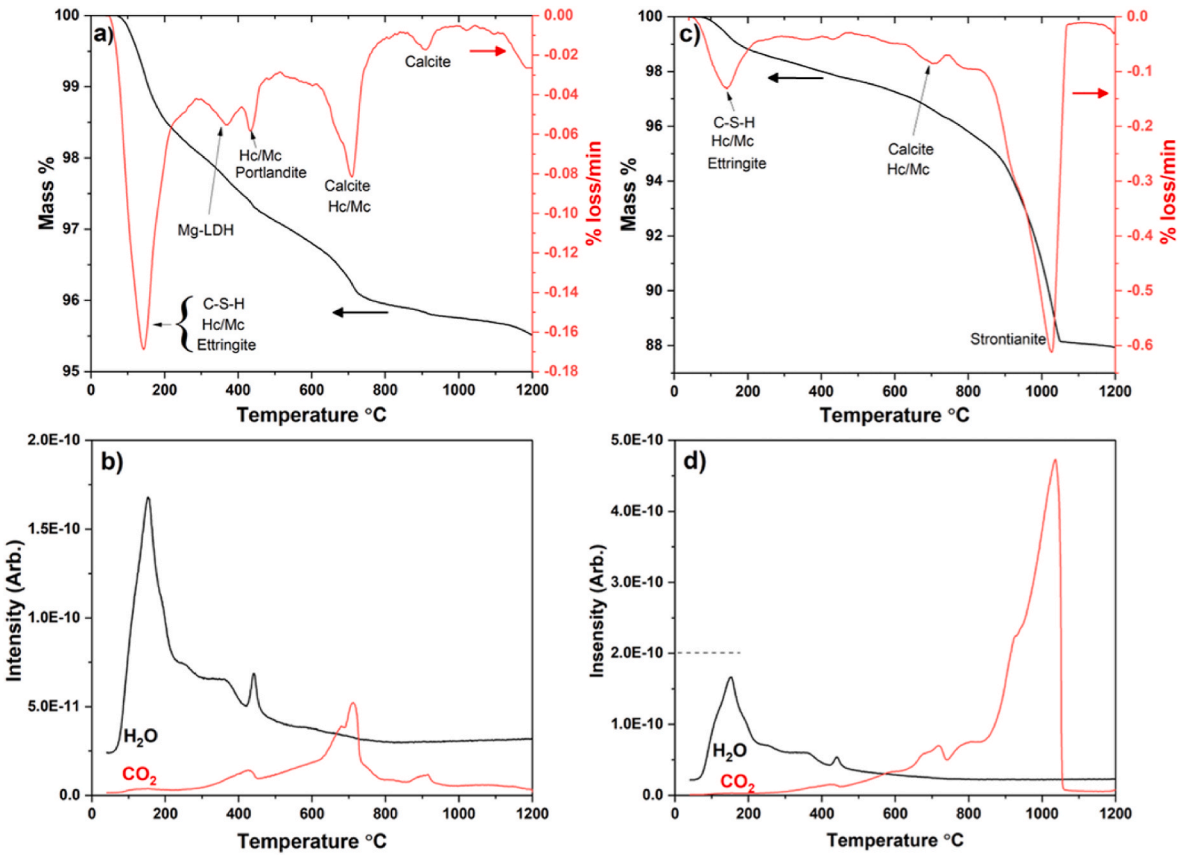

Fig. 2. TG/DTG-MS plots for samples cured at 20 °C for 1 day at 0 wt% SrCO3 a) TG/DTG and b) MS and, for 30 wt% $SrCO_3$ c) TG/DTG and d) MS (n.b. increased scale in c) and d)). Hc: Hemicarbonate, Mc: Monocarbonate, Mg-LDH: Hydrotalcite-like layered double hydroxide.

since calcite is a common material blended into commercial cement products. $CaCO_3$ typically affects cement hydration via partial reaction, and competition with sulfates for aluminium released during clinker hydration, resulting in the formation of calcium monocarboaluminate ($Ca_4Al_2(CO_3)(OH)_{12}{\cdot}5H_2O$), referred to as monocarbonate hereafter. This can lead to the stabilisation of ettringite ($Ca_6Al_2(SO_4)_3(OH)_{12}{\cdot}26H_2O$), which would otherwise typically slowly convert to calcium monosulfoaluminate ($Ca_4Al_2(SO_4)(OH)_{12}{\cdot}6H_2O$), referred to as monosulfate hereafter, via further reaction with clinker aluminates [26,27]. Certain amounts of calcium hemicarboaluminate ($Ca_4Al_2(CO_3)_{0.5}(OH)_{13}{\cdot}5.5H_2O$), referred to as hemicarbonate hereafter, have been identified as a kinetically favoured intermediate phase, though this is not predicted to be thermodynamically stable [26–28]. Overall, the calcite reaction is limited by alumina availability for hemi/-monocarbonate formation [26], and by mobility of CO_3^{2-} within the pore solution. Similar results were observed for the reaction of dolomite ($CaMg(CO_3)_2$), but with more hydrotalcite ($Mg_6Al_2CO_3(OH)_{16}{\cdot}4H_2O$) formation due to increased Mg, which removes Al from the solution. At higher temperatures, dolomite reduces monosulfate content, partially stabilising ettringite due to the increase in hydrotalcite-like content [29].

The aim of this study was to investigate the effect of $SrCO_3$ within a blast furnace slag – Portland cement matrix, typical of that utilised within the nuclear industry. It may be expected that $SrCO_3$ should perform in a similar manner to $CaCO_3$ within a Portland cement, and blended Portland-slag system, though with reduced solubility. The affinity for carbonate trapped as $SrCO_3$, and aluminates within the cement clinker need to be understood, both at ambient and elevated temperatures to allow for the greater certainty necessary in nuclear waste management. To investigate this, simulant waste forms were fabricated with (30 wt%), and without the incorporation of $SrCO_3$. The simulant waste forms were cured at 20 °C and 60 °C with characterisation performed at varying time points to follow the phase evolution within the hardened products.

2. Experimental programme

A reference cement paste was produced comprising a 9:1 (by weight) ratio of ground granulated blast furnace slag (GGBS, Hanson Port Talbot) to Portland cement (PC, Hanson Ribblesdale Works CEM I) with a water to solids (w/s) ratio of 0.39 by weight, using deionised water. To assess the stability of $SrCO_3$ as a ^{14}C immobilisation matrix, an additional mix was produced where 30 wt% of the cementitious powder (GGBS + PC) was replaced with $SrCO_3$, produced at the same w/s ratio of 0.39 using deionised water ($SrCO_3$, Fisher Scientific, 97.5% purity). The cement pastes were produced using a Heidolph RZR 2020 overhead mixer, with powders added into water, mixing for a fixed time of 5 min in batch sizes of 200 g per formulation (as shown in Table 1). Both mixes were cast into multiple 15 mL centrifuge tubes (then sealed with screw lids), with each batch split into two sub-batches, curing at 20 °C and 60 °C to determine if any radiogenic heating or heat from emplacement in a disposal facility would affect carbonate stability. For each testing time point (1 day, 7 days, 28 days and 90 days curing), a single centrifuge tube for each condition (4x conditions) was removed, and sectioned and/or crushed according to characterisation needs.

Solid monolith samples for SEM (scanning electron microscopy) analysis were prepared by sectioning samples using a diamond wafering blade, mounting within epoxy resin, grinding and polishing using sequentially finer grit paper and diamond pastes to a 1 μm finish. SEM samples were taken at 28 and 90 days curing, with samples analysed within 24–28 h after demoulding (delayed due to sectioning, mounting and polishing). This deviation from sampling time to analysis was

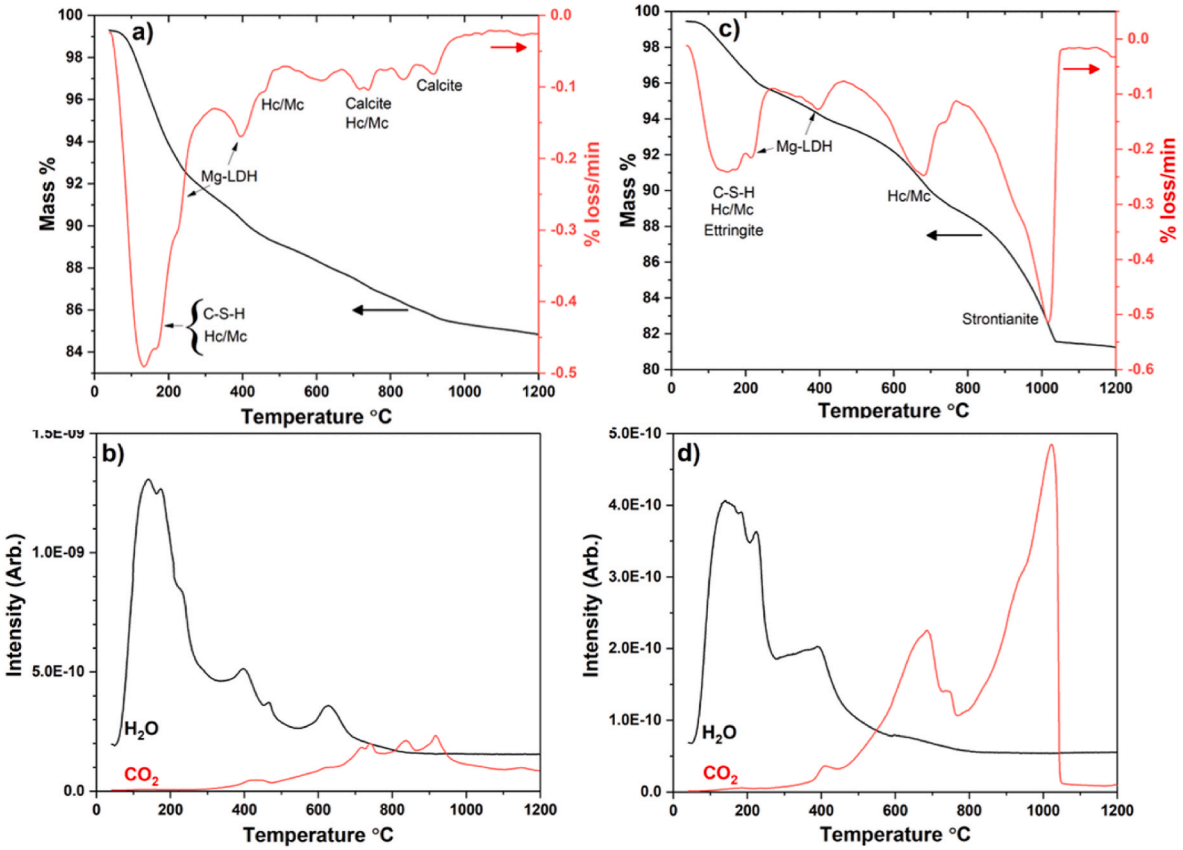

Fig. 3. TG/DTG-MS curved for samples cured at 20 °C for 90 days. 0 wt% SrCO3 a) TG/DTG and b) MS, 30 wt% SrCO3 c) TG/DTG and d) MS (n.b. increased scale in c) and d)). Hc: Hemicarbonate, Mc: Monocarbonate, Mg-LDH: Hydrotalcite-like layered double hydroxide.

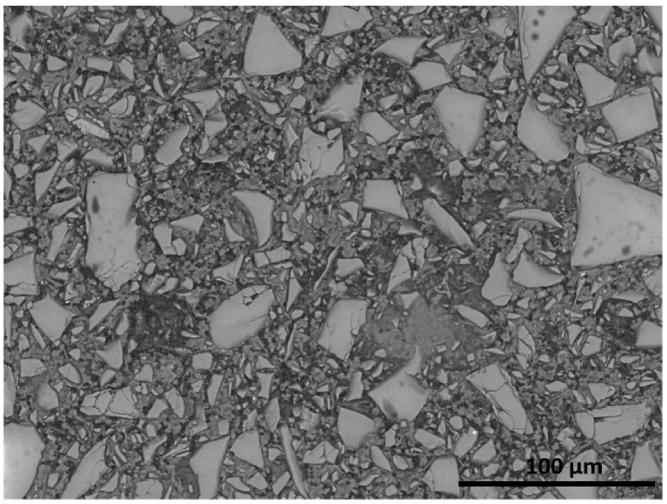

Fig. 4. Scanning electron micrograph of the 0 wt% $SrCO_3$ sample after curing at 20 °C for 90 days.

unavoidable for these samples due to the detailed preparation, however, this only results in a maximum of <5% deviation from the stated sampling time. Samples were analysed using a Hitachi TM3030 Scanning Electron Microscope (SEM), with a Bruker Quantax 70 Energy Dispersive X-ray Spectrophotometer (EDX). Micrographs were collected in backscattered electron mode (BSE) with a 15 kV accelerating voltage.

Ground samples were prepared for XRD (X-ray diffraction) and TG-MS (thermogravimetry-mass spectrometry) analysis. Unlike the solid samples, these were crushed at the required timepoints, and immediately immersed into acetone for 48 h, to arrest hydration. Samples were dried following the immersion, and ground to a fine powder using an agate pestle and mortar for further analysis. XRD was performed using a Bruker D2 PHASER diffractometer (Ni-filtered Cu Kα 1.5418 Å), with data collected between $5° \leq 2\theta \leq 60°$, with a step size of 0.01° and a 1 s dwell per step. TG-MS was performed using a Netzsch STA 449 F3 Jupiter utilising a QMS 403 D Aëolos mass spectrometer, using nitrogen as a carrier gas. Samples were held at 40 °C for 30 min under flowing nitrogen to remove any absorbed water, prior to beginning the thermal program. After which, samples were heated at 10 °C min^{-1} from 40 to 1200 °C in alumina crucibles.

2.1. Thermodynamic modelling

The thermodynamic modelling was performed using GEM-Selektor v3.6 (GEMS) [30,31], using the CEMDATA18 database [32]. The solid, liquid and gaseous phases used, along with thermodynamic data and points of departure from the reference database, are provided in the Supplementary Information (Tables S1–S3).

Our modelling utilised the degree of hydration values for this Portland cement clinker minerals and GGBS (utilising the sample precursor material and GGBS replacement levels) up to 360 days, as determined by Prentice et al. [33]. The key differences between these two experiments were curing temperature and water to solid ratio (w/s). In the Prentice et al. study, a w/s of 0.35 and curing temperature of 35 °C were used, which will alter the degree of hydration, but not to a significant degree for long-term hydration (curing time ≥28 days). Therefore, assuming these are the inputs of the degree of hydration in the $SrCO_3$-free and $SrCO_3$ containing systems, these inputs should be adequate for estimating the degree of hydration within these systems, given the identical mineralogical composition of the precursor cement and slag.

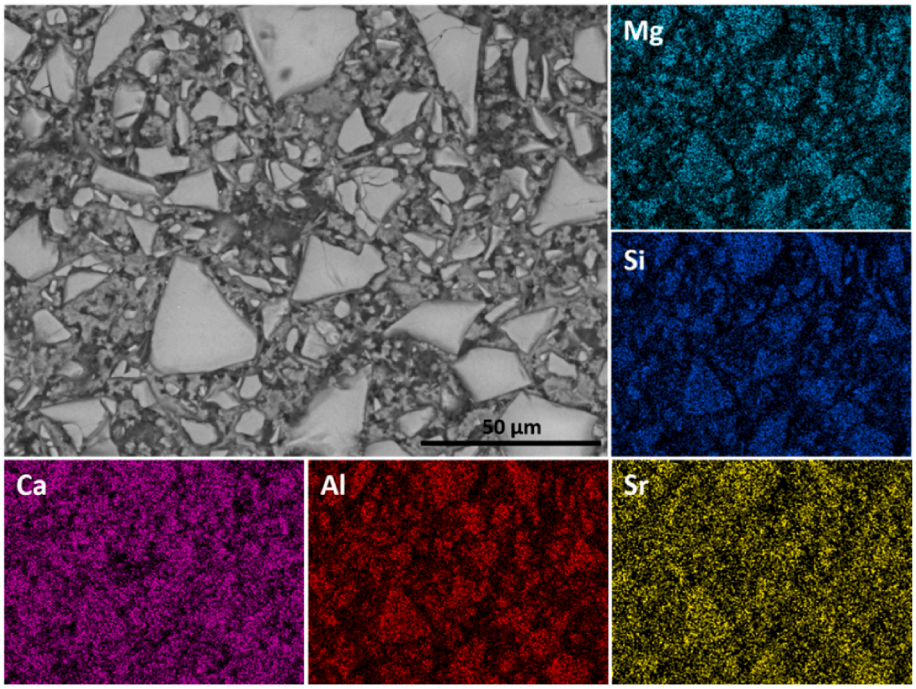

Fig. 5. Scanning electron micrograph and elemental maps (at higher magnification) of the 0 wt% $SrCO_3$ sample after curing at 20 °C for 90 days.

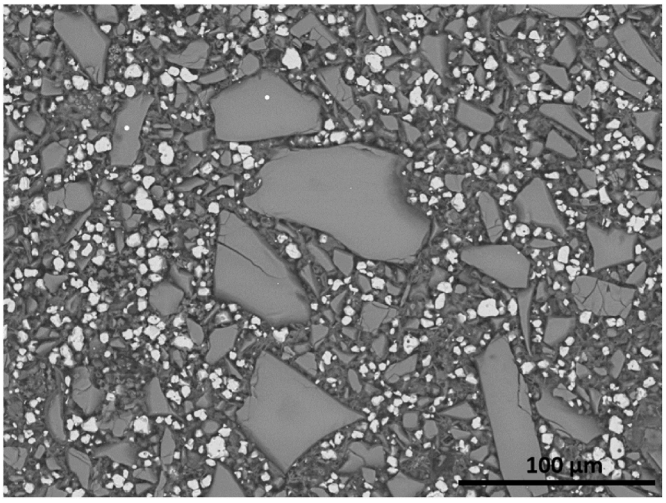

Fig. 6. Scanning electron micrograph of the 30 wt% $SrCO_3$ sample after curing at 20 °C for 90 days.

Activity coefficients for the aque ous species were determined via the Truesdell-Jones extension of the Debye-Hückel equation (Eq. (1)) [34]:

$$log_{10}\gamma_i = \frac{-A_\gamma z_i^2\sqrt{I}}{1+\dot{a}B_\gamma\sqrt{I}} + b_\gamma I + log_{10}\frac{X_{jw}}{X_w} \quad 1$$

Here, γ_i and z_i are the activity coefficient and charge of the i^{th} aqueous species respectively, A_γ and B_γ are temperature and pressure dependent coefficients, I is the molal ionic strength, X_{jw} is the molar quantity of water, and X_w is the total molar amount of the aqueous phase. A common ion size parameter, $\dot{a}$ (3.67 Å) and short-range interaction parameter, b_γ (0.123 kg/mol), were used, treating KOH as the background electrolyte [34,35].

CEMDATA18 mineral phases are recorded at standard conditions (298 K and 1 atm), therefore temperature corrections for the apparent Gibbs energy of formation, $\Delta_a G^0_{T_0}$, of these minerals are required to extrapolate to the temperatures of interest, T. Integration of the heat capacity function (Eq. (2)) is used in GEMS [36–38]:

$$\Delta_a G^0_{T_0} = \Delta_f G^0_{T_0} - S^0_{T_0}(T-T_0) - \int_{T_0}^{T}\int_{T_0}^{T}\frac{C^0_p}{T}dTdT \quad 2$$

$$= \Delta_f G^0_{T_0} - S^0_{T_0}(T-T_0) - a_0\left(Tln\frac{T}{T_0} - T + T_0\right) - a_1(T-T_0)^2$$

$$-a_2\frac{(T-T_0)}{2T\bullet T_0^2} - a_3\frac{\left(\sqrt{T}-\sqrt{T_0}\right)^2}{\sqrt{T_0}}$$

Where $\Delta_f G^0_{T_0}$ is the standard Gibbs energy of formation, $S^0_{T_0}$ is the standard absolute entropy at $T_0 = 298$ K, and C^0_p is the standard heat capacity, where a_0, a_1, a_2, and a_3 are the empirical coefficients of the heat capacity equation $C^0_p = a_0 + a_1T + a_2T^{-2} + a_3T^{-0.5}$. The apparent Gibbs free energy of formation, $\Delta_a G^0_{T_0}$, refers to the free energies of the elements and $S^0_{T_0}$ is the standard absolute entropy at $T_0 = 298$ K.

Due to the high proportion of Sr within this system, it was decided to utilise the ECSH model within CEMDATA18 in Table S1 (alongside other thermodynamic data) [32], to account for the potential for Sr substitution within C–S–H. A consequence of this is the limitation of the current ECSH model which does not allow for Al substitution within the C–S–H, which is likely to be significant due to the high proportion of slag. Utilising a C-(N-)A-S-H model which allows for Al substitution would, however, disregard the possibility for Sr uptake by C–S–H (which in turn might affect $SrCO_3$ dissolution). We expect the ECSH model to result in increased Al availability for AFm phase formation, and increased $SrCO_3$ dissolution – making this the potentially more conservative model, in terms of long-term durability, for these specific conditions. A series of hydrotalcite-like solid solution models (MAH, MAcH and MAsH [39]) replaced the OH-hydrotalcite and MA-OH-LDH model found within CEMDATA18 to better represent the magnesium aluminate hydrate (M-A-H) phase. The solid thermodynamic data are summarised in S1. Aqueous and gaseous phases included within this study are summarised in Tables S2 and S3, respectively.

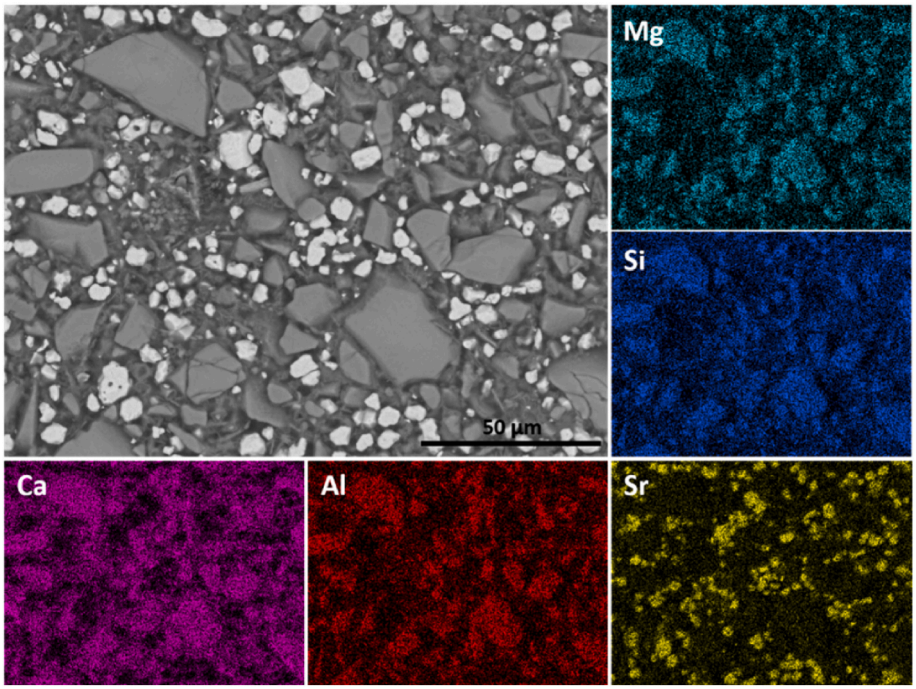

Fig. 7. Scanning electron micrograph and elemental maps (at higher magnification) of the 30 wt% $SrCO_3$ sample after curing at 20 °C for 90 days.

3. Results and discussion

3.1. Ambient temperature (20 °C) curing

The cementitious materials cured at 20 °C appeared and behaved similar to a conventional PC blended cement while being physically handled, demoulded, and prepared for analysis. The phase composition was determined by XRD, at curing times of 1, 7, 28 and 90 days (Fig. 1). Fig. 1 revealed a conventional slag-PC hydration for the 0 wt% $SrCO_3$ samples, as expected [33,40]. Within the first day, principal reflections revealed the formation of ettringite ($Ca_6Al_2(SO_4)_3(OH)_{12}{\cdot}26H_2O$) and hemicarbonate ($Ca_4Al_2(CO_3)_{0.5}(OH)_{13}{\cdot}5.5H_2O$). This was accompanied by partially unreacted clinker phases (alite (Ca_3SiO_5) and belite (Ca_2SiO_4)), calcite ($CaCO_3$), and possibly a small amount of monocarbonate ($Ca_4Al_2(CO_3)(OH)_{12}{\cdot}5H_2O$) or Mg–Al layered double hydroxide (LDH – e.g. Meixnerite ($Mg_6Al_2(OH)_{16}(OH)_2{\cdot}4H_2O$)), though reflections for these latter two phases were weak and overlapping, and therefore they cannot be independently differentiated here. The Mg–Al layered double hydroxide formed in blended Portland-slag or alkali activated slag systems is typically described as 'hydrotalcite-like' ($Mg_6Al_2CO_3(OH)_{16}{\cdot}4H_2O$), however with a formulation much closer to Meixnerite ($Mg_6Al_2(OH)_{16}(OH)_2{\cdot}4H_2O$) due to likely incorporation of OH^- in the interlayer, rather than CO_3^{2-} [41–43]. Thermal analysis of the 1 day cured 0 wt% $SrCO_3$ sample (Fig. 2 a, b) agreed with the phases observed via XRD analysis (Fig. 1), but also further underlined that phase formation was still an ongoing process. Typically, at <200 °C, there is a high proportion of weight loss associated with loss of water from C–S–H (poorly crystalline calcium silicate hydrate, the main strength forming phase and key product formed from clinker hydration), but also from overlapping ettringite, hemi/monocarbonate, and layered double hydroxide dehydration, making it difficult to differentiate these signals. A <2% mass loss was observed up to 200 °C, indicating that these phases, and C–S–H in particular, was only poorly developed – to be expected at an early age of hydration. The mass loss observed between 200 and 400 °C was assigned to the decomposition of layered double hydroxides, followed by portlandite decomposition (and additional hemi/monocarbonate dehydroxylation) at 400–450 °C. Mass loss between 600 and 1200 °C was ascribed to the loss of CO_2 from calcite (either as ground addition to the PC, or carbonation of the clinker/slag during storage) and from the decarbonation of mono/hemicarbonate, both of which only contributed to ~1% mass loss in Fig. 2 a,b [29, 44–49].

By day 7 most clinker phase reflections were reduced, indicating continued reaction of these phases over time (as typical of Portland cements). This was further evidenced by the emergence of portlandite ($Ca(OH)_2$) and a poorly crystalline reflection associated with C–S–H centred $2\theta = \sim 29°$ [50,51]. The principal reflection for ettringite disappeared by day 7, with a concurrent emergence of reflections associated with monosulfate ($Ca_4Al_2(SO_4)(OH)_{12}{\cdot}6H_2O$), while reflections for hemicarbonate, monocarbonate and hydrotalcite-like LDH all remained visible. With continued curing through 28 days and up to 90 days, the phase assemblage continued to change, with increasing intensity of reflections for monocarbonate and hydrotalcite-like LDH, and the continued presence of hemicarbonate reflections. The decreased reflection intensity for portlandite, along with the commensurate increase in relative intensity observed for hydrotalcite-like LDH was indicative of continued slag dissolution (providing Mg for hydrotalcite-like LDH formation) and C–S–H formation [52]. This change in phase assemblage was also apparent in the thermal analysis of the 90 day 0 wt% $SrCO_3$ sample (Fig. 3 a, b), with increased mass loss associated with water from C–S–H, hemi/monocarbonate and hydrotalcite-like LDH when compared to that observed after 1 day of curing (Fig. 2 a, b).

The addition of $SrCO_3$ to these binders appeared to result in some minor, but noticeable changes to the phase assemblage, as shown in Fig. 1. Due to the large number of strong reflections for $SrCO_3$ (strontianite), weak reflections from other mineral phases (especially if predominantly at $2\theta > 35°$) may not be observed due to overlapping reflections. After curing for 1 day, the differences (aside from $SrCO_3$ content) between the two samples (0 wt% and 30 wt% $SrCO_3$) were relatively minor and were associated with increased relative intensity for the ettringite and hemi/monocarbonate reflections (in the 30 wt% sample). Thermal analysis (Fig. 2c and d) of the 30 wt% $SrCO_3$ sample revealed a broadly similar mass loss, with initial decomposition of C–S–H, hemi/monocarbonate and ettringite, then continued slow water loss from the hydrated phases (hydrotalcite-like, portlandite, hemi/

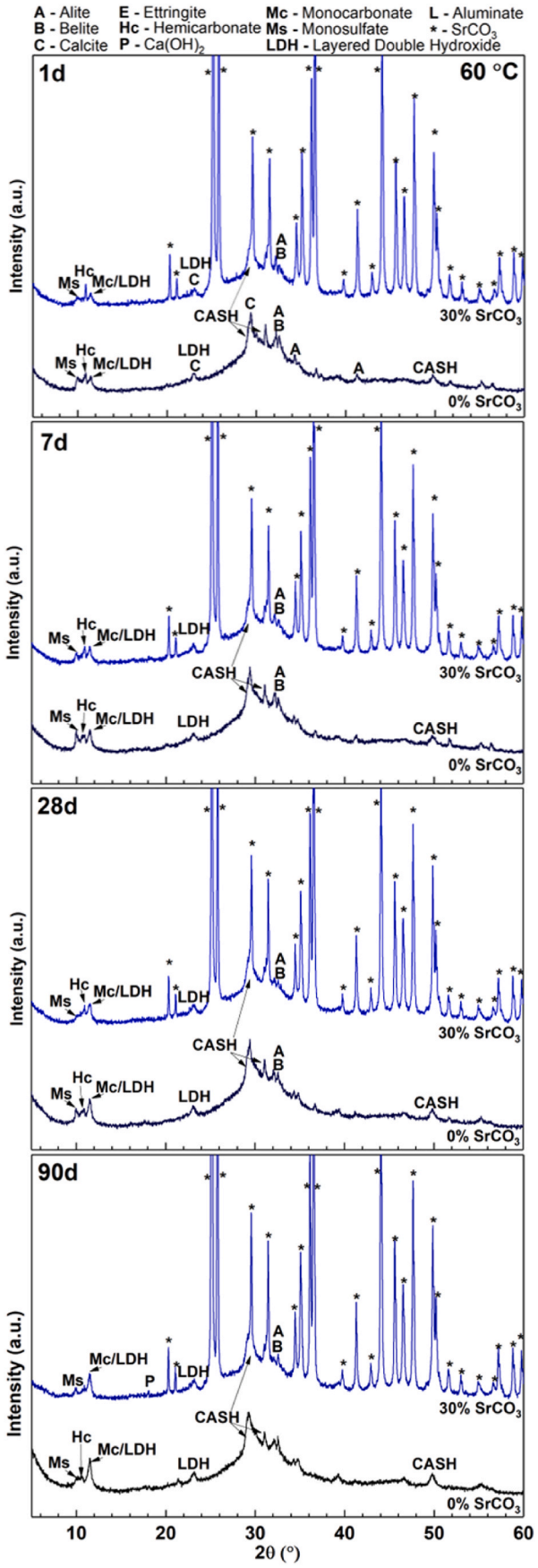

Fig. 8. X-ray diffraction patterns of samples cured at 60 °C from 1 day through to 90 days.

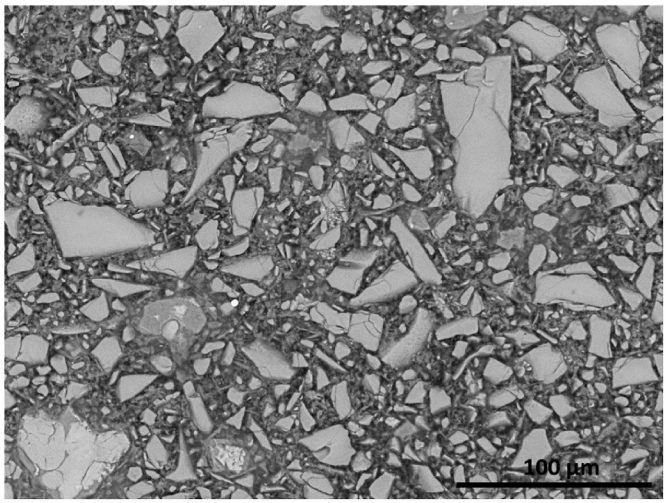

Fig. 9. Scanning electron micrograph of the 0 wt% $SrCO_3$ sample after curing at 60 °C for 90 days.

monocarbonate), up to ~800 °C when substantial decomposition of $SrCO_3$ occurred, as evidenced by the strong signal for CO_2 and associated mass loss.

The key difference between the 30 wt% $SrCO_3$ and 0 wt % $SrCO_3$ was the apparent stabilisation of ettringite in the former, which was evident from day 7 up to day 90. This observation was reinforced by the absence of any monosulfate reflections within the $SrCO_3$ containing sample, which indicated that sulfate remained bound within the ettringite phase. Alongside this, there appeared to be a slightly more intense reflection for hemicarbonate, and a less intense portlandite reflection. The formation of a C–S–H gel was observed, though partially overlapping with a strong strontianite reflection, with a poorly crystalline reflection centred at $2\theta = 29°$ appearing by day 7 of curing (though likely to occur before but was much less prominent at 1 day of curing). Thermal analysis of the 30 wt% $SrCO_3$ sample at 90 days curing (Fig. 3 c, d) revealed clear changes compared to the 0 wt% $SrCO_3$ sample. There was a reduced mass loss at <200 °C (3.3% mass loss with $SrCO_3$ addition, compared to 7.1% without), with a visibly reduced DTG (differential thermal gravimetry) signal at ~150 °C which largely corresponds to C–S–H, indicating reduced C–S–H formation. Hydrotalcite-like was still present, releasing water at ~220 °C and 400 °C, in addition to $SrCO_3$ which released CO_2 between 800 and 1000 °C. Most noticeably, in comparison to the 0 wt% $SrCO_3$ sample, there was a greatly increased mass loss centred at ~600 °C releasing CO_2, which was attributed to decomposition of hemi/monocarbonate. This demonstrates that the reaction of $SrCO_3$ with clinker aluminates involves the formation of carbonated AFm phases.

Typically in Portland cement blends, tricalcium aluminate ($Ca_3Al_2O_6$) within the clinker reacts with sulfates added into the cement during manufacture (e.g. gypsum or anhydrite) to form ettringite (Equation (3)), which subsequently reacts with more tricalcium aluminate to form monosulfate (Equation (4)) [53,54]. However, carbonate additions (e.g. $CaCO_3$), can promote the formation of carbonated AFm phases (such as hemi- and mono-carbonate) resulting in the preferential formation of these from clinker aluminates, instead of reaction with ettringite [26,27]. Formation of hemi- and mono-carbonates also increases the SO_3/Al ratio within the pore solution, with both effects stabilising ettringite [55]. The continued presence of ettringite in the 30% $SrCO_3$ samples is considered to be the result of $SrCO_3$ partially reacting, leading to the stabilisation of ettringite, and preventing the conversion to monosulfate.

$$Ca_3Al_2O_6 + 3(CaSO_4{\cdot}2H_2O) + 26H_2O \rightarrow Ca_6Al_2(SO_4)_3(OH)_{12}{\cdot}26H_2O \quad 3$$

$$Ca_6Al_2(SO_4)_3(OH)_{12}{\cdot}26H_2O + 2(Ca_3Al_2O_6) + 4H_2O \rightarrow 3(Ca_4Al_2(SO_4)(OH)_{12}{\cdot}6H_2O) \quad 4$$

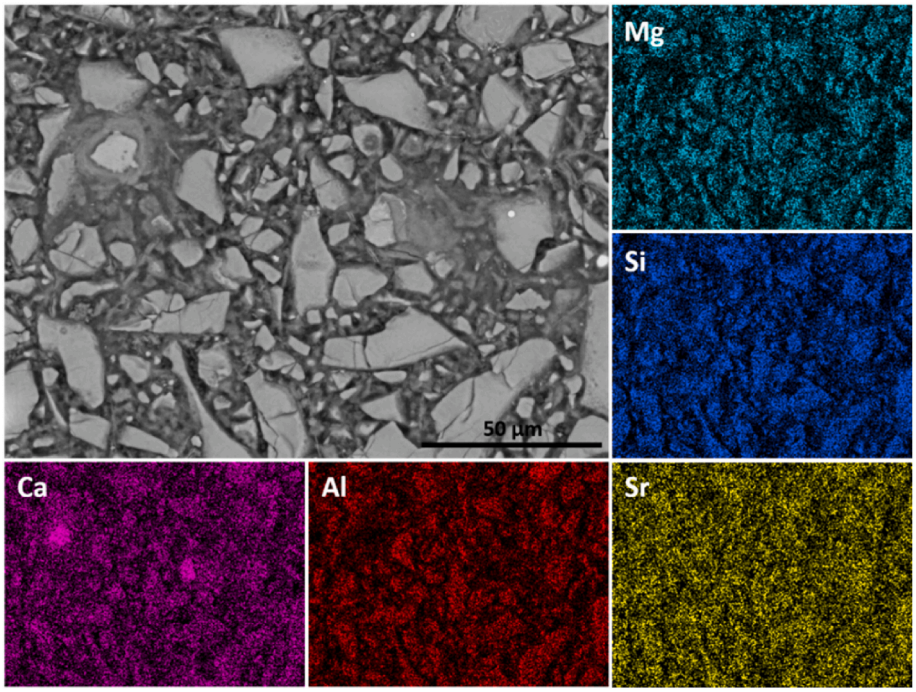

Fig. 10. Scanning electron micrograph and elemental maps (at higher magnification) of the 0 wt% $SrCO_3$ sample after curing at 60 °C for 90 days.

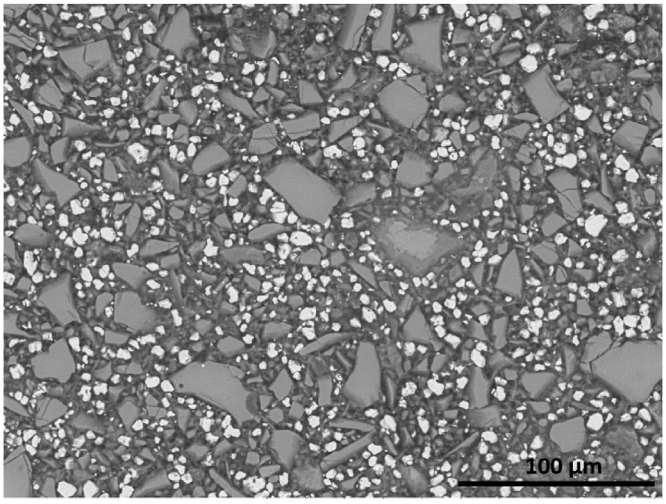

Fig. 11. Scanning electron micrograph of the 30 wt% $SrCO_3$ sample after curing at 60 °C for 90 days.

SEM micrographs and EDX maps of the 0% $SrCO_3$ sample at 90 days curing (Figs. 4 and 5) revealed a conventional slag-Portland cement microstructure, with angular particles of unreacted slag intertwined within a C–S–H binder. This is typical of UK nuclear cements containing such a high proportion (9:1 mix GGBS:PC) of slag, with much slag remaining unreacted [33,41]. At higher magnification in Fig. 5, the elemental maps confirm the imaging observations – angular slag particles (particularly enriched in Mg and Si), with a distribution of Ca, Al and Si throughout the matrix. The Sr map has been shown to retain ease of comparison with the $SrCO_3$ containing samples. The apparent signal within Fig. 5 EDX map is from slightly overlapping emission lines from Si ($K_{\alpha1} = 1.740$ eV) and Sr ($L_{\alpha1} = 1.806$ keV), rather than indication of Sr within the sample. A narrower window was selected for Sr, but some overlap from Si K_α emission was still observed.

The SEM-EDX micrographs (Figs. 6 and 7) for the 30 wt% $SrCO_3$ samples were similar to those of the 0 wt% samples, except for the large amount of unreacted $SrCO_3$ indicated by the very bright particles dispersed throughout the matrix. At higher magnification (Fig. 7) these solid particles of $SrCO_3$ do not reveal any obvious reaction rims (at this magnification) or migration of Sr away from the $SrCO_3$ particles (though a background signal from overlap with Si does give rise to a weak signal apparent throughout). No cracks can be seen emanating from the SrCO3 particles, suggesting these have overall been successfully encapsulated by the GGBS:PC matrix.

From both the XRD data, and electron microscopy analysis the immobilisation of $SrCO_3$ does not result in any deleterious microstructural or chemical reactions which would affect structural integrity (e.g. expansive phase formation) within a 90 day period at a curing temperature of 20 °C, other than the formation of minor amounts of carbonated AFm phases and stabilisation of ettringite from reaction with $SrCO_3$.

3.2. Elevated temperature (60 °C) curing

Increasing the curing temperature to 60 °C resulted in formation of the same product phases as observed when curing at 20 °C, although in different relative proportions (Fig. 8) for both the 0 wt% and 30 wt% $SrCO_3$ samples. At early ages (1d and 7d) there were lower intensity reflections associated with the unreacted clinker phases, and reflections for monosulfate, hemicarbonate, monocarbonate and hydrotalcite-like LDH were also observed, together with a reflection centred at $2\theta = 29°$, characteristic of a poorly crystalline C–S–H phase. These changes were expected since curing at 60 °C will accelerate reactivity at early ages. Similar to the 20 °C cured material, the reflections associated with strontianite were still present in the 30 wt% $SrCO_3$ sample cured at 60 °C. Of most significance is the absence of ettringite in the 30 wt% $SrCO_3$ sample cured at 60 °C (dissimilar to the 20 °C 0 wt% $SrCO_3$ sample), which is consistent with the observation of more intense reflections for monosulfate at both 1- and 7-days curing times. This was not unexpected because ettringite is often noted to be less stable above 50 °C, leading to the preferential formation of monosulfate [38,56]. Unfortunately, this precludes using the absence of ettringite as a proxy for $SrCO_3$ dissolution, as we postulated for the 20 °C samples.

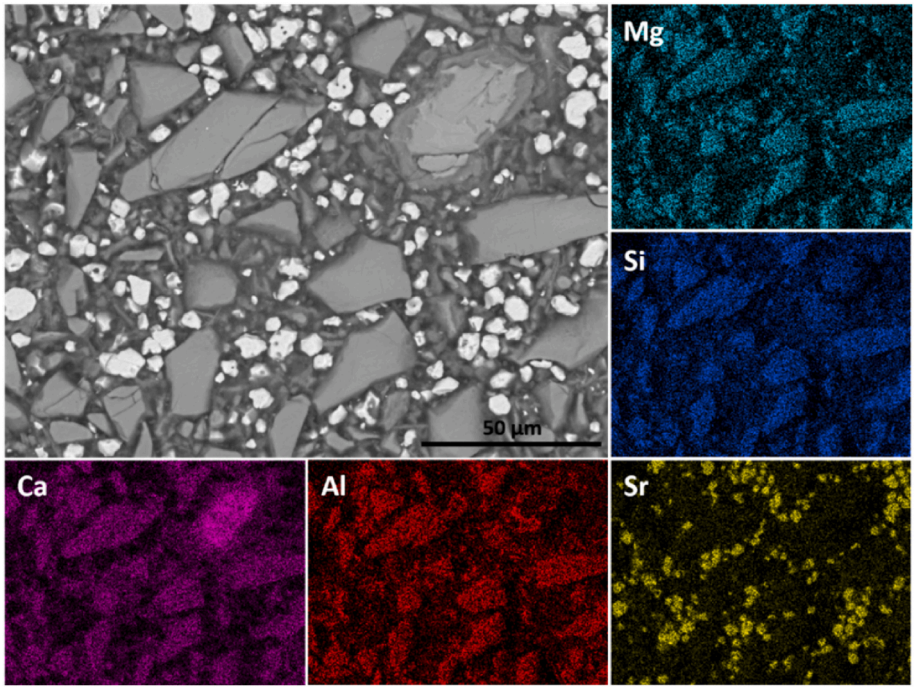

Fig. 12. Scanning electron micrograph and elemental maps (at higher magnification) of the 30 wt% $SrCO_3$ sample after curing at 60 °C for 90 days.

From 28 days through to 90 days curing the relative proportions of monosulfate and hemicarbonate decreased in both the 0 wt% and 30 wt % $SrCO_3$ samples, commensurate with increasing relative intensities for monocarbonate reflections. We postulate this finding based on the secondary hydrotalcite-like LDH reflection at $2\theta = 23–24°$ which remains essentially constant at all curing time points. Therefore, the observed increase of intensity of the primary hydrotalcite-like LDH reflection (that overlaps with monocarbonate) at $2\theta = \sim 12°$ could be attributed to the continued formation of monocarbonate.

SEM/EDX analysis of the 0 wt% $SrCO_3$ sample after 90 days curing at 60 °C (Figs. 9 and 10) revealed a conventional slag-Portland cement microstructure, with a large proportion unreacted slag remaining (fully expected with this high slag content; Table 1), interspersed within a calcium (aluminium) silicate rich binder indicative of a C–S–H gel. The Sr EDX map was included for comparison, indicating that a low background signal was present across the sample due to minor overlap of the Si Kα emission (rather than from the presence of Sr).

The addition of 30 wt% $SrCO_3$ into the matrix (Figs. 11 and 12) also afforded a conventional slag-Portland cement microstructure, however, with the addition of bright solid $SrCO_3$ particles which were uniformly scattered across the microstructure. The EDX map for Sr (Fig. 12) did not reveal any strong diffusion of Sr from the $SrCO_3$ particles, which appeared to be well encapsulated within the cementitious system.

The samples cured at 60 °C did not show any chemical or microstructural changes which would indicate any deleterious reactions (aside from a potential increase in carbonate AFm phases) in good agreement with the samples cured at 20 °C. No deleterious expansive phases were formed and there was no obvious cracking or shrinkage observable from the microstructure. It can therefore be surmised that up to 30 wt% $SrCO_3$ has been successfully incorporated within these GGBS: PC cement matrices, up to at least 90 days curing.

3.3. Thermodynamic modelling

The results of phase and microstructure analysis by XRD and SEM-EDX indicated limited reaction occurred as a result of $SrCO_3$ incorporation. The strongest evidence of a reaction thus far is the apparent stabilisation of ettringite at 20 °C with additions of $SrCO_3$, indicative of some limited reactivity, along with increasing formation of mono/hemicarbonates identified via thermal analysis. To determine whether the identified phases are likely to be thermodynamically stable, or are merely transient kinetically favoured phases, thermodynamic modelling was undertaken using GEMSelektor for the samples containing $SrCO_3$. Data are presented up to 90 days in Fig. 13(a) and Fig. 14(a), corresponding to the maximum age observed experimentally, and further extended in Figs. 13(b) and Figure 14(b) up to 360 days, to gain an appreciation of the longer-term phase stability.

The results of the simulations are depicted graphically in terms of grams of hydrates per 100g of solid reactant (or precursors). The mass of solids in the phase diagram will increase above 100g initially due to phase formation with water. For the 20 °C cured sample, the first 90 days fully predicted the formation of the phases identified within XRD analysis of the physical samples (Fig. 1), with clinker and slag reacting to form a C–S–H phase, ettringite, monocarbonate and hydrotalcite-like LDH. A small quantity of portlandite, monosulfate and hemicarbonate were predicted as transient phases. From day 36 up to day 360, no new phases were predicted with only the slow continued hydration of GGBS: PC (indicated by the increasing hydrotalcite-like LDH contribution). A very minor quantity (3.3%) of the $SrCO_3$ was predicted to react (changing the $SrCO_3$ content from 30g/100g solid reactants to 29g/100g after 360 days), with the bulk remaining unreacted.

The difference between predicted and observed phases (particularly the predicted transient phases) can be explained by both limitations of the thermodynamic simulations, and the more limited kinetics of the physical cementitious system. Particularly, this simulation predicts transient phase formation, followed by the disappearance of hemicarbonate (with a subsequently larger formation of monocarbonate). Within the observed XRD patterns (Fig. 1), hemicarbonate was still visible after 90 days curing at 20 °C. This difference between the simulation and experimental determination is likely due to the lower mobility of carbonates within the physical cement, which is limited by the granularity of the $SrCO_3$, by required mobility within the pore solution, and the kinetics of formation. Hemicarbonate has been found as a kinetically favoured intermediate phase when $CaCO_3$ is added to cements [26–28]. Furthermore, due to the estimated degree of reaction of the GGBS, the CO_2/Al_2O_3 ratio of the simulation may be higher than

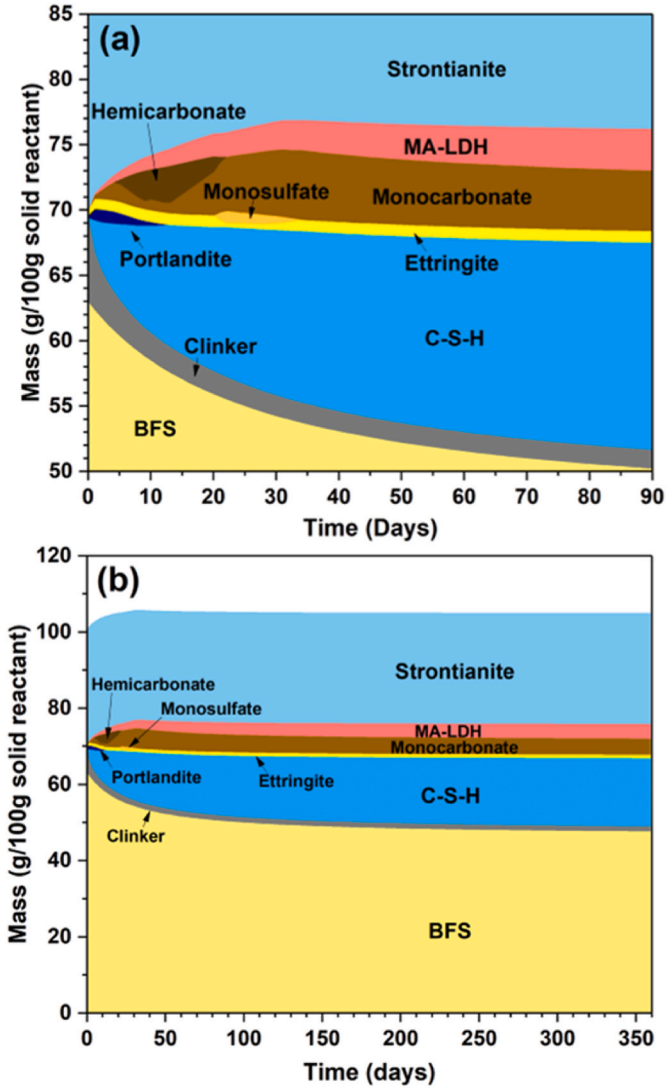

Fig. 13. Thermodynamic simulations of predicted phase assemblages at 20 °C, (a) first 90 days, (b) up to 360 days.

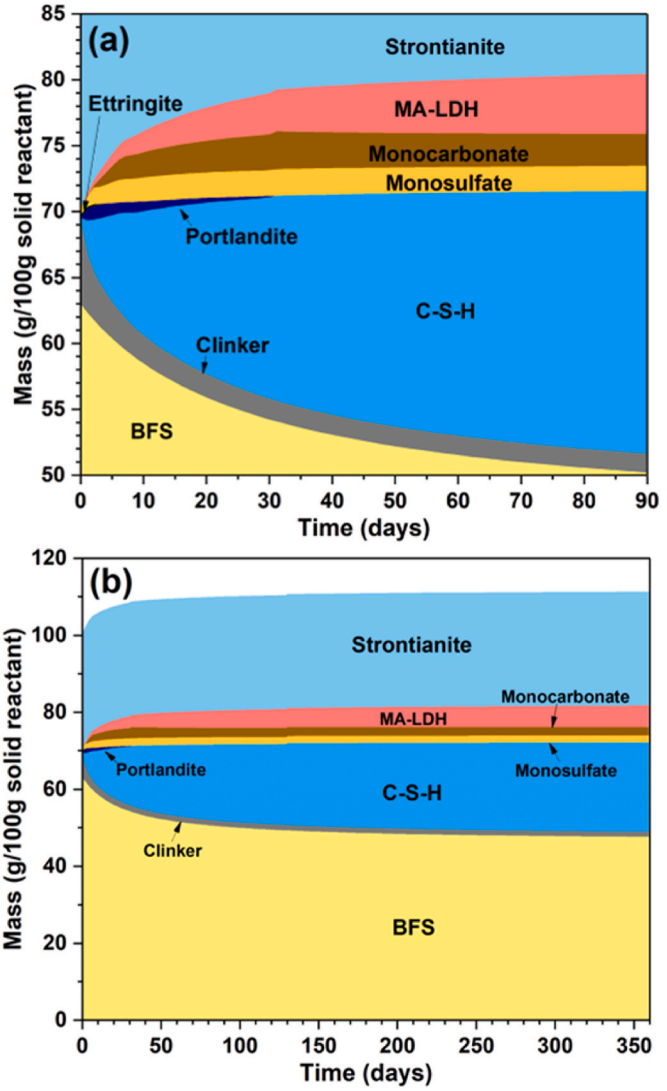

Fig. 14. Thermodynamic simulations of predicted phase assemblages at 60 °C, (a) first 90 days, (b) up to 360 days.

what was occurring in the system which realised the formation of monocarbonate in place of hemicarbonate in the simulation. It is likely, therefore, that monocarbonate will be the ultimate phase formed at the expense of hemicarbonate, but equilibrium was not reached by 90 days.

Simulation of the system at the elevated curing temperature of 60 °C (Fig. 14(a) and (b)) predicted a similar phase assemblage to that observed experimentally (Fig. 2), with a few minor points of difference. The simulation predicted the formation of a C–S–H gel concurrent with dissolution of the GGBS and clinker phases, alongside the formation of monosulfate, monocarbonate and hydrotalcite-like LDH in agreement with Fig. 2. Ettringite was predicted to form initially, but disappearing by day 2 concurrent with monosulfate formation. Another transient phase predicted to form almost immediately was portlandite, which disappeared by day 36. There remains a large quantity of unreacted strontianite throughout the simulated time periods, with only 1.3% of the $SrCO_3$ predicted to react (changing the $SrCO_3$ content from 30g/100g solid reactants to 29.6g/100g after 360 days). The modelling for the 60 °C system was in broad agreement with the observed phase assemblage in that no appreciable quantity of ettringite was predicted to form, apart from very transiently (up to day 2) before a rapid conversion to monosulfate. Hemicarbonate was not predicted to form, but was experimentally observed (Fig. 2), although the major X-ray reflections for hemicarbonate appeared to slowly decrease in intensity from 1 day to 90 days curing. Similar to the predicted phase assemblages at 20 °C, this difference between model and experimentally determined is anticipated to be due to kinetic limitations within the physical cement matrix, with monocarbonate likely to predominate at later ages.

4. Conclusions

In this study, we demonstrated that a substantial quantity of strontium carbonate ($SrCO_3$) can be effectively immobilised within a blast furnace slag – Portland cement blend, with only minor reactivity, following a reaction pathway and phase formation similar to those encountered for Portland cements blended with $CaCO_3$. Phase analysis and microstructural investigation revealed a typical PC-GGBS matrix consisting of C–S–H, hemi/monocarbonate, hydrotalcite-like, ettringite/monosulfate and unreacted slag particles, all encapsulating particles of $SrCO_3$. A minor reaction with $SrCO_3$ occurred leading to the formation of carbonated AFm phases (hemicarbonate and monocarbonate), and resulting in stabilisation of ettringite. The formation of hemicarbonate alongside monocarbonate within the cement systems was indicative of a kinetic lag between thermodynamic predictions and the physical samples, perhaps due to $SrCO_3$ particle size and consequent restricted carbonate mobility. This may ultimately result in further dissolution of $SrCO_3$ as hemicarbonate converts to monocarbonate, however,

monocarbonate was predicted to remain stable for at least the 360 days modelled, therefore this would not be expected to decompose and release ^{14}C into the environment under the timeframe modelled.

The reaction of $SrCO_3$ is therefore dependent on both carbonate mobility within the waste form (which would in turn be affected by precipitated particle size), and reaction with clinker aluminates to form carbonated AFm phases. This indicates that a higher incorporation of $SrCO_3$ could easily be tolerated (as the relative proportion of clinker aluminates to react would be reduced), up to the point at which incorporation severely reduces compressive and tensile strength (due to reduced cementitious content, and a larger proportion of filler). Conversely, variation of the cement to slag ratio (e.g. increasing the cement content) could potentially result in a higher proportion of reacted $SrCO_3$ due to more clinker aluminate reaction, resulting in a higher relative amount of carbonate AFm phases. The lower decomposition temperature (~200 °C lower) for both hemi- and monocarbonates compared to $SrCO_3$ should however be noted, as under fire accident conditions ^{14}C-AFm phases would release their radiocarbon inventory earlier than $Sr^{14}CO_3$.

The use of $SrCO_3$ as a ^{14}C host can be recommended over $BaCO_3$ or $CaCO_3$ due to both lower solubility, and lack of reactions with sulfates. No reactions between $SrCO_3$ and sulfate were observed (nor are they thermodynamically favourable under these conditions), whereas $BaCO_3$ reacts with sulfates to release carbonate. Although some $SrCO_3$ has reacted within the cement matrix, following a similar reaction path to $CaCO_3$, the lower aqueous solubility of $SrCO_3$ is likely to reduce this reaction and retain the ^{14}C inventory within $Sr^{14}CO_3$. Indeed, the slightly higher reactivity of $CaCO_3$ could be exploited through addition of a small fraction finely ground $CaCO_3$ into $SrCO_3$-GGBS:PC waste forms, with the aim to preferentially react $CaCO_3$ with clinker aluminates, therefore eliminating $SrCO_3$ reactions. Ultimately however, the long-term stability of any ^{14}C containing waste form would be dependent on repository conditions, particularly the composition and flow of any groundwater as well as the aqueous geochemistry over much longer timeframes, and interactions with backfill material.

Declaration of competing interest

The authors declare that they have no known competing financial interests or personal relationships that could have appeared to influence the work reported in this paper.

Data availability

Data will be made available on request.

Acknowledgements

The authors are grateful for funding provided for this project by EPSRC under grant EP/S032959/1 and partial support to University of Sheffield from the Horizon 2020-Euratom research and training programme 2020–2024 under grant agreement No. 945098. CLC is grateful to EPSRC for an Early Career Fellowship, under grant reference EP/N017374/1. This work was also supported by the National Research Foundation of Korea (NRF) grant funded by the Korean government (MSIP: Ministry of Science, ICT and Future Planning) (No. NRF-2019M2A7A1001811). We wish to acknowledge the Henry Royce Institute for Advanced Materials, funded through EPSRC grants EP/R00661X/1, EP/S019367/1, EP/P02470X/1 and EP/P025285/1 for the financial support. This research utilised the HADES/MIDAS facility at the University of Sheffield established with financial support from EPSRC and BEIS, under grant EP/T011424/1 [57].

Appendix A. Supplementary data

Supplementary data to this article can be found online at https://doi.org/10.1016/j.cemconcomp.2022.104823.

References

[1] International Energy Agency, Net Zero by 2050 - a Roadmap for the Global Energy Sector, IEA, 2021.
[2] Nuclear Decomissioning Authority, The Role of the Waste Hierarchy for Radioactive Waste, NDA, 2008.
[3] Secretary of State for the Environment, Review of Radioactive Waste Managment Policy - Final Conclusions, HMSO, UK, 1995.
[4] International Atomic Energy Agency, Status and Trends in Spent Fuel and Radioactive Waste Management, IAEA, 2018.
[5] International Atomic Energy Agency, Management of Waste Containing Tritium and Carbon-14, IAEA, 2004.
[6] M.-S. Yim, F. Caron, Life cycle and management of carbon-14 from nuclear power generation, Prog. Nucl. Energy 48 (1) (2006) 2–36.
[7] A. Grandjean, G. Leturcq, Natural sintering of carbonate powder for use as a carbon-14 immobilization matrix, J. Nucl. Mater. 345 (1) (2005) 11–18.
[8] A. Magnusson, K. Stenström, ^{14}C produced in Swedish nuclear power reactors - measurements on spent ion exchange resins, various process water systems and ejector off-gas, Svensk Kärnbränslehantering AB (SKB) (2005) 1–43. R-05-78.
[9] C. Bucur, I. Florea, P.E. Reiller, D. Dumitrescu, ^{14}C content in candu spent ion exchange resins and its release under alkaline conditions, Radiocarbon 60 (6) (2018) 1797–1808.
[10] D.L. Moir, K.J. Ross, J.D. Chen, A.W. Tarr, E.L. Bialas, W.A. Boivin, D.C. Doern, D. L. Hoffman, J.P.M. Ross, Determination of ^{14}C in spent moderator ion-exchange resin from bruce nuclear generating station A, J. Radioanal. Nucl. Chem. 185 (1) (1994) 69–81.
[11] J. Gray, A. Guest, ^{17}O and ^{18}O analysis of heavy water, Int. J. Rad. Appl. Instr. A. 37 (9) (1986) 969–971.
[12] W. Sohn, D.-W. Kang, J. Chi, Approaches for reducing carbon-14 stack emissions from Korean CANDU® nuclear power plant, J. Nucl. Sci. Technol. 41 (2) (2004) 235–246.
[13] Y.-K. Choi, S. An, D.-H. Kim, J.H. Cho, H.S. Park, H.J. Ahn, ^{14}C removal technology for the treatment of spent resin from nuclear power plants: a review, in: Transations of the Korean Nuclear Society Autumn Meeting, 2014. Pyongchang, Korea.
[14] S.-C. Park, H.-R. Cho, J.-H. Lee, H.-Y. Yang, O.-B. Yang, A study on adsorption and desorption behaviors of ^{14}C from a mixed bed resin, Nucl. Eng. Technol. 46 (6) (2014) 847–856.
[15] M.A. Hafeez, J. Jeon, S. Hong, N. Hyatt, J. Heo, W. Um, Fenton-like treatment for reduction of simulated carbon-14 spent resin, J. Environ. Chem. Eng. (2020), 104740.
[16] S.E. Beaty, Environmental impact of THORP - the philosophy, Energy Environ. 7 (3) (1996).
[17] P.I. Hudson, C.P. Buckley, Aerial and Liquid Effluent Treatment in BNFL's Thermal Oxide Reprocessing Plant (THORP), Proceedings of the first NUCEF international symposium, Ibaraki, Japan, 1995.
[18] C.A. Utton, E. Gallucci, J. Hill, N.B. Milestone, Interaction between $BaCO_3$ and OPC/BFS composite cements at 20 °C and 60 °C, Cem. Concr. Res. 41 (3) (2011) 236–243.
[19] P. Taylor, Solubility and Stability of Inorganic Carbonates: an Approach to the Selection of a Waste Form for Carbon-14, Atomic Energy of Canada Limited, 1987.
[20] G.L. Haag, Carbon-14 Immobilization via the CO_2-$Ba(OH)_2$ Hydrate Gas-Solid Reaction, 16th DOE nuclear air cleaning conference, San Diego, CA, 1980.
[21] N. Massoni, S. Le Gallet, Investigation of the sintering of barytocalcite with $BaCO_3$ as a secondary phase for immobilizing carbon-14, J. Nucl. Mater. 476 (2016) 13–19.
[22] R.D. Scheele, L.L. Burger, Selection of a Carbon-14 Fixation Form, PNL/DOE, 1982.
[23] B.K. Singh, M.A. Hafeez, H. Kim, S. Hong, J. Kang, W. Um, Inorganic waste forms for efficient immobilization of radionuclides, ACS ES&T Engineering 1 (8) (2021) 1149–1170.
[24] Radioactive Waste Management (RWM), Geological Disposal: Generic Disposal Facility Design, RWM, 2016.
[25] D.R. Lide, CRC Handbook of Chemistry and Physics, 88th Edition, CRC Press, Boca Raton, FA, 2007.
[26] M. Zajac, A. Rossberg, G. Le Saout, B. Lothenbach, Influence of limestone and anhydrite on the hydration of Portland cements, Cem. Concr. Compos. 46 (2014) 99–108.
[27] B. Lothenbach, G. Le Saout, E. Gallucci, K. Scrivener, Influence of limestone on the hydration of Portland cements, Cement Concr. Res. 38 (6) (2008) 848–860.
[28] T. Matschei, B. Lothenbach, F.P. Glasser, Thermodynamic properties of Portland cement hydrates in the system CaO-Al_2O_3-SiO_2-$CaSO_4$-$CaCO_3$-H_2O, Cement Concr. Res. 37 (10) (2007) 1379–1410.
[29] M. Zajac, S.K. Bremseth, M. Whitehead, M. Ben Haha, Effect of $CaMg(CO_3)_2$ on hydrate assemblages and mechanical properties of hydrated cement pastes at 40 °C and 60 °C, Cement Concr. Res. 65 (2014) 21–29.
[30] D.A. Kulik, T. Wagner, S.V. Dmytrieva, G. Kosakowski, F.F. Hingerl, K. V. Chudnenko, U.R. Berner, GEM-Selektor geochemical modeling package: revised algorithm and GEMS3K numerical kernel for coupled simulation codes, Comput. Geosci. 17 (1) (2013) 1–24.
[31] T. Wagner, D.A. Kulik, F.F. Hingerl, S.V. Dmytrieva, GEM-Selektor geochemical modeling package: TSolMod library and data interface for multicomponent phase models, Can. Mineral. 50 (5) (2012) 1173–1195.

[32] B. Lothenbach, D.A. Kulik, T. Matschei, M. Balonis, L. Baquerizo, B. Dilnesa, G. D. Miron, R.J. Myers, Cemdata18: a chemical thermodynamic database for hydrated Portland cements and alkali-activated materials, Cement Concr. Res. 115 (2019) 472–506.
[33] D.P. Prentice, B. Walkley, S.A. Bernal, M. Bankhead, M. Hayes, J.L. Provis, Thermodynamic modelling of BFS-PC cements under temperature conditions relevant to the geological disposal of nuclear wastes, Cement Concr. Res. 119 (2019) 21–35.
[34] H.C. Helgeson, D.H. Kirkham, G.C. Flowers, Theoretical prediction of the thermodynamic behavior of aqueous electrolytes by high pressures and temperatures; IV, Calculation of activity coefficients, osmotic coefficients, and apparent molal and standard and relative partial molal properties to 600 degrees C and 5kb, Am. J. Sci. 281 (10) (1981) 1249–1516.
[35] A. Vollpracht, B. Lothenbach, R. Snellings, J. Haufe, The pore solution of blended cements: a review, Mater. Struct. 49 (8) (2016) 3341–3367.
[36] T. Matschei, F.P. Glasser, Temperature dependence, 0 to 40°C, of the mineralogy of Portland cement paste in the presence of calcium carbonate, Cement Concr. Res. 40 (5) (2010) 763–777.
[37] D. Damidot, B. Lothenbach, D. Herfort, F.P. Glasser, Thermodynamics and cement science, Cement Concr. Res. 41 (7) (2011) 679–695.
[38] B. Lothenbach, T. Matschei, G. Möschner, F.P. Glasser, Thermodynamic modelling of the effect of temperature on the hydration and porosity of Portland cement, Cement Concr. Res. 38 (1) (2008) 1–18.
[39] D.P. Prentice, L. Gomez-Zamorano, M. Balonis, B. Erdemli, K. Ellison, N. Neithalath, D. Simonetti, G. Sant, The effects of (di-,tri-valent)-cation partitioning and intercalant anion-type on the solubility of hydrotalcites, J. Am. Ceram. Soc. 103 (10) (2020) 6025–6039.
[40] C.R. Wilding, The performance of cement based systems, Cement Concr. Res. 22 (2–3) (1992) 299–310.
[41] R. Taylor, I.G. Richardson, R.M.D. Brydson, Composition and microstructure of 20-year-old ordinary Portland cement-ground granulated blast-furnace slag blends containing 0 to 100% slag, Cement Concr. Res. 40 (7) (2010) 971–983.
[42] M. Ben Haha, B. Lothenbach, G. Le Saout, F. Winnefeld, Influence of slag chemistry on the hydration of alkali-activated blast-furnace slag - Part I: effect of MgO, Cement Concr. Res. 41 (9) (2011) 955–963.
[43] I.G. Richardson, S. Li, Composition and structure of an 18-year-old 5M KOH-activated ground granulated blast-furnace slag paste, Construct. Build. Mater. 168 (2018) 404–411.
[44] V.R.L. Constantino, T.J. Pinnavaia, Basic properties of $Mg^{2+1-x}Al^{3+x}$ layered double hydroxides intercalated by carbonate, hydroxide, chloride, and sulfate anions, Inorg. Chem. 34 (4) (1995) 883–892.
[45] W. Tongamp, Q. Zhang, F. Saito, Preparation of meixnerite (Mg-Al-OH) type layered double hydroxide by a mechanochemical route, J. Mater. Sci. 42 (22) (2007) 9210–9215.
[46] G. Villain, M. Thiery, G. Platret, Measurement methods of carbonation profiles in concrete: thermogravimetry, chemical analysis and gammadensimetry, Cem. Concr. Res. 37 (8) (2007) 1182–1192.
[47] G.T. Faust, Thermal analysis studies on carbonates I. Aragonite and calcite, Am. Mineral. 35 (3) (1950) 207–224.
[48] B.Z. Dilnesa, B. Lothenbach, G. Le Saout, G. Renaudin, A. Mesbah, Y. Filinchuk, A. Wichser, E. Wieland, Iron in carbonate containing AFm phases, Cement Concr. Res. 41 (3) (2011) 311–323.
[49] N.C. Collier, Transition and decomposition temperatures of cement phases - a collection of thermal analysis data, Ceram.-Silik. 60 (4) (2016) 338–343.
[50] E. L'Hôpital, B. Lothenbach, G. Le Saout, D. Kulik, K. Scrivener, Incorporation of aluminium in calcium-silicate-hydrates, Cement Concr. Res. 75 (2015) 91–103.
[51] R.J. Myers, E. L'Hôpital, J.L. Provis, B. Lothenbach, Effect of temperature and aluminium on calcium (alumino)silicate hydrate chemistry under equilibrium conditions, Cement Concr. Res. 68 (2015) 83–93.
[52] B. Lothenbach, K. Scrivener, R.D. Hooton, Supplementary cementitious materials, Cement Concr. Res. 41 (12) (2011) 1244–1256.
[53] I. Odler, Hydration, setting and hardening of Portland cement, in: P.C. Hewlett (Ed.), Lea's Chemistry of Cement and Concrete, Butterworth Heinemann, Oxford, UK, 2003, pp. 241–297.
[54] J.W. Bullard, H.M. Jennings, R.A. Livingston, A. Nonat, G.W. Scherer, J. S. Schweitzer, K.L. Scrivener, J.J. Thomas, Mechanisms of cement hydration, Cement Concr. Res. 41 (12) (2011) 1208–1223.
[55] T. Matschei, B. Lothenbach, F.P. Glasser, The AFm phase in Portland cement, Cement Concr. Res. 37 (2) (2007) 118–130.
[56] B. Lothenbach, F. Winnefeld, C. Alder, E. Wieland, P. Lunk, Effect of temperature on the pore solution, microstructure and hydration products of Portland cement pastes, Cement Concr. Res. 37 (4) (2007) 483–491.
[57] N.C. Hyatt, C.L. Corkhill, M.C. Stennett, R.J. Hand, L.J. Gardner, C.L. Thorpe, The HADES facility for high activity decommissionining engineering & science: part of the UK national nuclear user facility, IOP Conf. Ser. Mater. Sci. Eng. 818 (2020), 012022.